Reviews in Mineralogy & Geochemistry
Vol. 72 pp. 971-996, 2010

Theoretical Computation of Diffusion in Minerals and Melts

Nico de Koker
Bayerisches Geoinstitut
Universität Bayreuth, Germany
nico.dekoker@uni-bayreuth.de

Lars Stixrude
Department of Earth Sciences
University College London, United Kingdom
l.stixrude@ucl.ac.uk

INTRODUCTION

Chemical diffusion is a fundamental process in the evolution of planets. Equilibration within and among phases in response to changes in physical conditions requires the comprising chemical species to be spatially rearranged, over distances comparable to the grain size. Quantitative description of such processes demands diffusivities of these chemical species to be accurately known, while detailed insight into the mechanisms of diffusion at the atomic scale elucidate their dependence on pressure, temperature and composition.

By applying our understanding of chemical bonding in condensed systems to numerically simulate diffusivity over a range of pressures and temperatures of planetary interest, we can obtain direct constraints on diffusivities at these extreme conditions, and self consistently assess the models used to extrapolate experimental data. Such computations further serve as a proving ground for testing the robustness of the various levels of theory applied in the characterization of bonding and dynamics of a material.

The mathematical description of diffusion was first developed in the context of thermal transport by Fourier (1822). Its applicability to chemical transport was recognized by Fick (1855), who cast Fourier's law of thermal conduction in terms of chemical transport and applied it to experiments on the diffusion of salt in a column of water. In an anisotropic system of n components, Fick's description is most generally given by

$$\frac{\partial c_A}{\partial t} = \sum_{i,j}^{3}\sum_{B}^{n-1} - D_{AB}^{ij}\frac{\partial^2 c_B}{\partial x_i \partial x_j} \tag{1}$$

where c_A is the concentration of species A, and D_{AB}^{ij} is the relevant component of the diffusivity matrix (e.g., Crank 1975; Lasaga 1998; Zhang 2010). However, this description of diffusion is entirely in the continuum limit, and does not give any insight into the mechanisms by which chemical transport occurs at the atomic level.

The description of chemical diffusivity was cast in an atomistic context by studies of Brownian motion (Einstein 1905; Smoluchowski 1906; Langevin 1908; Chandrasekhar 1943), which was described as colloidal particles undergoing stochastic migrations, punctuated by instantaneous elastic collisions. The Stokes-Einstein relation between particle diffusivity and fluid viscosity derived from this works well for simple liquids such as metals (Poirier 1988;

1529-6466/10/0072-0022$05.00 DOI: 10.2138/rmg.2010.72.22

Dobson et al. 2000), but discrepancies for fluids of more complex composition suggests that diffusion involves mechanisms not captured by such a simple model (Zhang 2008).

Computer-aided atomistic simulation has made an enormous contribution to statistical mechanics and condensed matter physics. Early work coincided with the development of computers as tools for numerical analysis, with Metropolis et al. (1953) using the MANIAC at Los Alamos National Laboratory to calculate the equation of state of a periodic system of hard disks (two dimensional hard spheres), using the Monte Carlo method that now bears his name. This work was soon followed by a Monte Carlo calculation of the equation of state of a Lennard-Jones fluid (Wood and Parker 1957), molecular dynamics simulations of the fluid-solid transition in a system of hard spheres (Alder and Wainwright 1957), and molecular dynamics simulation of a Lennard-Jones system to compute the chemical diffusivity of liquid Argon (Rahman 1964).

The groundwork for first-principles methods was set in place with the development of density functional theory (DFT; Hohenberg and Kohn 1964; Kohn and Sham 1965), which steadily increased in popularity throughout the 1970s as an effective tool for characterizing electronic structure and bonding in simple solids. Car and Parrinello (1985) combined DFT with the formalism of molecular dynamics in a computation of the physical properties of crystalline silicon, representing the first dynamical application of electronic structure based computations and pointing the way to direct first-principles treatment of fluids. Today, computational resources are sufficient for more accurate Born-Oppenheimer molecular dynamics (Payne et al. 1992) to be readily performed for systems of relatively complex chemical composition.

The purpose of this review is to introduce the condensed matter physics used in performing atomistic simulations, together with the statistical mechanics applied in its analysis to determine diffusivities. To illustrate these methods we will discuss a selection of applications of atomistic modeling to the characterization of diffusivity in both liquids as well as in solids.

THEORETICAL FOUNDATIONS

Thermodynamic description

As an irreversible process, diffusion is readily described in the framework of non-equilibrium thermodynamics. Consider a system of N particles, each one of n compounds, at pressure P and temperature T. The system has volume V, entropy S and chemical potentials μ_A, μ_B,…, μ_n. By the Euler equation the internal energy for the system is

$$E = TS - PV + \sum_{A}^{n} \mu_A N_A \tag{2}$$

Diffusion will result in entropy production of

$$\left(\frac{\partial S}{\partial t}\right)_{P,T,N} = -\frac{1}{T}\sum_{A}^{n} \mathbf{J}_A \cdot \nabla \mu_A \tag{3}$$

Where $\mathbf{J}_A$ is the mass flux and $\nabla\mu/T$ its conjugate force. $\mathbf{J}_A$ is a vector giving the number of particles of component A passing through a unit surface in a unit time

$$\mathbf{J}_A(t) = m_A \sum_{a_A}^{N_A} \dot{\mathbf{R}}_{a_A}(t) \tag{4}$$

where m_A and $\dot{\mathbf{R}}_{a_A}(t)$ is respectively the mass and velocity of particle A, with the over-score dot denoting a time derivative.

Conservation of mass requires

$$\sum_{A}^{n} \mathbf{J}_A = 0 \tag{5}$$

so that only $n-1$ flux vectors are independent. A similar argument applies to the chemical potentials due to the Gibbs-Duhem relation. Forming a Taylor expansion of the mass flux in terms of its conjugate force, and assuming the chemical potential does not vary strongly with position, we have

$$\mathbf{J}_A = -\frac{1}{T}\sum_{B}^{n-1} L_{AB}\nabla\mu_B \tag{6}$$

where L_{AB} are the $n-1 \times n-1$ independent components of the symmetric phenomenological matrix (Onsager 1931a,b). In an anisotropic material, each of these components is itself a second rank tensor in spatial components.

Laboratory measurements as well as computational simulations of diffusion are more readily characterized in terms of concentration gradients than chemical potentials. Applying the chain rule to Equation (6), we may also write

$$\mathbf{J}_A = -\sum_{B}^{n-1} D_{AB}\nabla c_B \tag{7}$$

where c_B is the concentration of component B, and D_{AB} are the $n-1 \times n-1$ independent components of the diffusivity matrix given by

$$D_{AB} = \frac{1}{T}\sum_{C}^{n-1} \frac{\partial\mu_C}{\partial c_B} L_{AB} \tag{8}$$

Note that unlike the phenomenological matrix, the diffusivity matrix is not symmetrical.

In describing $\mathbf{J}$ it is important to define a spatial frame of reference, relative to which the flux occurs. If $\dot{\mathbf{R}}_A$ is the velocity of species A with concentration c_A, the corresponding mass flux is

$$\mathbf{J}_A = c_A\left(\dot{\mathbf{R}}_A - \dot{\mathbf{R}}_0\right) \tag{9}$$

where $\dot{\mathbf{R}}_0$ is the reference velocity.

For a constant number of particles with velocities described relative to an absolute reference frame independent of particle distribution (the system described in Eqns. 2-8), the reference frame is referred to as *mass-fixed* or *barycentric* (de Groot and Mazur 1969; Lasaga 1998). This choice is most amenable to theory, and relevant to molecular dynamics simulations. In contrast, across coexisting phase boundaries or compositional couples, diffusion is described relative to the phase/couple interface, which moves in response to the flux (Kirkendall effect; Smigelskas and Kirkendall 1947), with regions further from the interface serving as chemical reservoirs. In this *volume-fixed reference frame* the flux is weighted by the partial molar volume $\overline{V}_A$ of each component A in the mass conservation condition

$$\sum_{A}^{n} \overline{V}_A \mathbf{J}_A = 0 \tag{10}$$

In order to transform the diffusivity matrix between these reference frames one applies the coordinate transformation (de Groot andMazur 1969)

$$D^V_{AB} = D_{AB}\left(\delta_{AB} + \frac{\overline{V}_A}{\overline{V}_N}\frac{c_A}{c_N}\right) \tag{11}$$

where D^V_{AB} is the diffusivity in the volume fixed reference frame.

D_{AB} is generally referred to as the *chemical diffusivity matrix*, the diagonal components are the *main-*, *diagonal-* or *self-diffusivities*[1], with off-diagonal components known as *off-diagonal-* or *cross-diffusivities*. When the off-diagonal diffusivities are comparable in magnitude to the diagonal values, changes in concentration of one component will strongly affect the distribution of the other components. In stable phases, the eigenvalues of the diffusivity matrix are all positive, but in unstable systems some eigenvalues of the matrix are negative, resulting in diffusion against the concentration gradient, also referred to as *uphill diffusion*. Unmixing of fluids and exsolution in minerals are example scenarios which involve uphill diffusion (e.g., Lasaga 1998; Zhang 2008).

In the foregoing discussion we assumed that the only force experienced by diffusing particles is due to the chemical potential. Should other forces be present (electromagnetic, gravity, etc.) these can be incorporated by additional terms in the Euler equation describing the force-potential conjugate pair (Lasaga 1979; Callen 1985).

Statistical mechanical description

Diffusion in liquids. The statistical mechanical description of diffusion was placed on a sound theoretical platform during the 1950s with the development of linear response theory (Callen and Welton 1951; Green 1952; Kubo 1957; Zwanzig 1965). The response function formalism allows the diffusivity, inherently a non-equilibrium property, to be expressed in terms of the time evolution of an equilibrium system

$$D_A = \frac{1}{3N_A}\sum_{a_A}^{N_A}\int_0^\infty \left\langle \dot{\mathbf{R}}_{a_A}(t)\cdot\dot{\mathbf{R}}_{a_A}\right\rangle dt \tag{12}$$

where

$$\left\langle \dot{\mathbf{R}}_{a_A}(t)\cdot\dot{\mathbf{R}}_{a_A}\right\rangle = \lim_{t_0\to\infty}\frac{1}{t_0}\int_0^{t_0}\dot{\mathbf{R}}_{a_A}(t)\dot{\mathbf{R}}_{a_A}(t+t')dt' \tag{13}$$

is the velocity autocorrelation function. It can be readily shown that

$$\frac{1}{3N_A}\sum_{a_A}^{N_A}\int_0^\infty \left\langle \dot{\mathbf{R}}_{a_A}(t)\cdot\dot{\mathbf{R}}_{a_A}\right\rangle dt = \lim_{t\to\infty}\frac{\left\langle \left|\mathbf{R}_A(0)-\mathbf{R}_A(t)\right|^2\right\rangle}{6t} \tag{14}$$

which then yields the result obtained by Einstein (1905), Smoluchowski (1906) and Langevin (1908) in their studies of Brownian motion

$$D_A = \lim_{x\to\infty}\frac{\left\langle \left|\mathbf{R}_A(0)-\mathbf{R}_A(t)\right|^2\right\rangle}{6t} \tag{15}$$

with $\langle|\mathbf{R}_A(0) - \mathbf{R}_A(t)|^2\rangle$ the mean square displacement of the particle; Equation (15) is known as the Einstein relation (Hansen and McDonald 2006; Allen and Tildesley 1987).

A more general description is given by the mass flux correlation function, in terms of which the full phenomenological coefficient matrix is (Zhou and Miller 1996; Wheeler and Newton 2004)

$$L_{AB} = \frac{1}{3k_{\mathrm{B}}V}\int_0^\infty \left\langle \mathbf{J}_A(t)\cdot\mathbf{J}_B\right\rangle dt \tag{16}$$

with the diffusivity matrix following via Equation (8).

1 Although the self-diffusivity is often defined in terms of gradients in isotopic concentrations, it is standard in computational work to use the term for the diagonal values of the diffusivity matrix, denoting these simply as D_A. We will follow this convention in this chapter as well.

Shear viscosity is similarly given by the average of the stress autocorrelation function

$$\eta = \frac{V}{3k_{\mathrm{B}}T}\sum_{i\neq j}\int_0^\infty \left\langle \sigma_{ij}(t)\sigma_{ij}\right\rangle dt \tag{17}$$

where σ_{ij} are the off-diagonal components of the stress tensor. This relation allows one to directly compute the liquid viscosity, rather than relying on simple scaling relations between D and η, such as the Stokes-Einstein (Einstein 1905; Langevin 1908) or Eyring relations (Eyring 1936).

Diffusion in solids. In contrast to liquids, solid-state diffusion is generally much slower and anisotropic. Migration occurs by individual jumps of atoms into either vacancies or interstitial sites, which are associated with activation energies of several eV. For typical vibrational frequencies, the Boltzmann distribution predicts jumps to occur with characteristic times of 10^{-4}-10^{-9} seconds. We will consider vacancy self-diffusion here; the equations describing interstitial diffusion are very similar.

The rate and geometry of jump events depends on the crystal lattice, the nature (size, charge, etc.) of the migrating atom, and on the concentration of vacancies in the lattice. In addition to simple jumps of atoms into vacancies on their own sublattice, diffusion in solids can also involve cyclic mechanisms of multiple steps and combinations of jump events onto different sublattices. A common example, the six-jump cycle, is well known in alloys (Elcock 1959), and involves a set of six jump events by which an atom and a vacancy end up swapping positions (Fig. 1).

Figure 1. Schematic of the individual steps of the six jump cycle of solid-state diffusion. • and × denote two different chemical species, with • ultimately exchanging positions with a vacancy. This sequence of jumps is energetically more favorable than a single diagonal jump of • into the vacancy.

The self-diffusivity of component A migrating though vacancy diffusion is given by (e.g., Philibert 1991; Glicksman 2000)

$$D_A = X_A^{\mathrm{vac}} D_A^{\mathrm{vm}} \tag{18}$$

where X_A^{vac} is the molar fraction of vacancies on the A-site, and D_A^{vm} is the vacancy diffusivity. To evaluate D_A^{vm} we view the diffusion process as a reaction in which the system is activated from equilibrium to an activated state. In the activated state, the migrating atom will be at a saddle point on the potential energy surface corresponding to the highest potential energy it takes on during a migration event.

Let ν_{att} be the attempt frequency, which is simply the vibrational frequency of the atom in the direction of the candidate jump, and ν_{jump} the frequency with which these attempts result in successful jumps. By the Boltzmann distribution, the fraction of successful attempts is

$$\frac{\nu_{\mathrm{jump}}}{\nu_{\mathrm{att}}} = \exp\left(-\frac{G_A^{\mathrm{vm}}}{k_{\mathrm{B}}T}\right) = \exp\left(\frac{S_A^{\mathrm{vm}}}{k_{\mathrm{B}}}\right)\exp\left(-\frac{H_A^{\mathrm{vm}}}{k_{\mathrm{B}}T}\right) \tag{19}$$

where G_A^{vm}, H_A^{vm} and S_A^{vm} are respectively the Gibbs free energy, enthalpy and entropy of vacancy migration. The vacancy diffusivity can now be related to the attempt frequency via

$$D_A^{\mathrm{vm}} = \frac{f_{\mathrm{c}} Z\lambda^2}{6}\nu_{\mathrm{jump}} = \frac{f_{\mathrm{c}} Z\lambda^2}{6}\nu_{\mathrm{att}}\exp\left(\frac{S_A^{\mathrm{vm}}}{k_{\mathrm{B}}}\right)\exp\left(-\frac{H_A^{\mathrm{vm}}}{k_{\mathrm{B}}T}\right) \tag{20}$$

with Z is the coordination (i.e., the number of candidate jump directions) and λ is the jump

distance. f_c is a correlation factor accounting for the possibility that, following a successful jump, the atom can jump back into its previous position. The value of f_c depends on the crystal structure, varying between 0.5 and 1.0 (Borg and Dienes 1988; Shewmon 1989). H_A^{vm} is the height difference on the potential energy surface between the equilibrium and saddle points, while S_A^{vm} can be shown from transition state theory (Vinyard 1957) to be

$$\exp\left(\frac{S_A^{vm}}{k_B}\right) = \frac{\prod_{i=1}^{3N} \nu_i}{\nu_{att} \prod_{i=1}^{3N-1} \nu_i'} \tag{21}$$

where N is the number of atoms in the system, ν_i and ν_i' are phonon frequencies at the equilibrium position and at the saddle point respectively, and the product in the denominator excludes the unstable mode frequency associated with the migration.

The *intrinsic* vacancy fraction can be obtained as

$$X_A^{vac} = \exp\left(-\frac{G_A^{vf}}{k_B T}\right) = \exp\left(\frac{S_A^{vf}}{k_B}\right)\exp\left(-\frac{H_A^{vf}}{k_B T}\right) \tag{22}$$

with G_A^{vf}, S_A^{vf}, and H_A^{vf} respectively the Gibbs free energy, entropy and enthalpy of vacancy formation. H_A^{vf} is the energy difference between a perfect, infinite lattice and an infinite lattice containing a single vacancy. The difference in configurational entropy between the perfect and imperfect lattices is negligible, so that S_A^{vf} is given by the differences in vibrational entropy between the two geometries as (Burton 1972; Gillan and Jacobs 1983)

$$\exp\left(\frac{S_A^{vf}}{k_B}\right) = \frac{\prod_{i=1}^{3N} \nu_i}{\prod_{i=1}^{3N} \nu_i'} \tag{23}$$

Note that the assumption in these formulas is that the crystal contains no trace element impurities, i.e., all vacancies are *intrinsic*. If these are of different charge than the ion they substitute, additional vacancies are required in order for charge balance to be maintained. Indeed, the concentration of such *extrinsic* impurities are often much higher than intrinsic vacancies, so that X_A^{vac} can be estimated from the trace element concentration instead.

COMPUTATIONAL APPROACHES

Atomistic simulation involves the numerical investigation of materials by applying the principles of condensed matter theory to characterize bonding and dynamics. Used wisely, these computational techniques afford understanding of macroscopic material properties in the context of behavior at the atomic level.

A variety of methods exist, each suited to investigating a specific subset of physical properties. Important considerations in choosing a suitable technique of simulation include the nature of the property of interest, whether thermal and/or electronic effects need to be characterized, the desired accuracy of the result, the quality and availability of experimental measurements, and the available computational resources. Commonly applied simulation techniques include static energy calculation, structural optimization, lattice dynamics, Monte Carlo computation, molecular dynamics, and electronic band structure determination. All these methods require as input the chemical composition, a reasonable initial geometry, and information on bonding via parameterized potentials or electronic structure.

We will begin by discussing various methods by which bonding can be characterized, and then consider methods through which thermal effects in materials can be simulated in more detail. This will lead us into a discussion of the various methods by which diffusivity may be computed and characterized.

Characterization of bonding

The physical conditions on and within Earth are such that bonding must be accurately characterized in order to capture the essential physics of condensed terrestrial phases (Birch 1952; Knopoff and Uffen 1954). Simple kinetic models that neglect bonding are not sufficient, and specialized descriptions either via parameterized potentials or directly by means of the electronic structure must be used.

Parameterized potential approach. Perhaps the simplest characterization of bonding involves describing interatomic interaction in terms of a set of analytical equations with parameters constrained from the known physics of the system of interest. A canonical example of such a potential is that due to Lennard-Jones (1924)

$$\nu^{\mathrm{LJ}}(x) = 4\varepsilon\left[\left(\frac{\sigma}{x}\right)^{12} - \left(\frac{\sigma}{x}\right)^{6}\right] \tag{24}$$

where ε represents the ground state potential energy and σ is a radial scaling parameter. By minimizing the misfit between properties computed using Equation (24) and experimental data for the system of interest (e.g., liquid Ar), optimal values for ε and σ can been determined. Numerous similar expressions exist by which the potential energy may be parameterized in terms of two-, three-, and four-body interactions (e.g., Gale 1998, 2001), common examples being the Born-Mayer, Buckingham, Morse and Stillinger-Weber functional forms. Such descriptions can consist of many free parameters, the accurate constraint of which requires large and preferably varied data sets for the materials in question.

Standard potential sets exist for some common materials such as water (Berendsen et al. 1987), silica (van Beest et al. 1990), and also silicate melts (Matsui 1994). While these potential sets may be used to compute physical properties in close agreement with experimental data, they give only atomistic insight, not electronic, and are severely limited in their predictive power when applied to conditions outside the range of chemical and/or physical conditions at which they were constrained.

First-principles approach. First-principles or *ab initio* calculations apply electronic structure theory to characterize bonding. The potential energy of the material associated with bonding is obtained *in situ* by computing the electronic structure of the material. Of the electronic structure-based methods that have been developed DFT remains the state of the art, and has been widely applied in the physical sciences.

In the standard quantum mechanical formalism embodied by the time independent Schrödinger equation

$$\hat{\mathcal{H}}\Psi = \mathcal{E}\Psi \tag{25}$$

representation of bonding requires characterization of the total electronic energy $\mathcal{E}$ and wave function Ψ for the Hamiltonian of the system of interest

$$\hat{\mathcal{H}} = -\frac{\hbar^2}{2m_{\mathrm{e}}}\nabla^2 + \mathcal{V}(\mathbf{r}_1, \mathbf{r}_2, \ldots, \mathbf{r}_{N_{\mathrm{e}}}, \mathbf{R}_1, \mathbf{R}_2, \ldots, \mathbf{R}_{N_{\mathrm{n}}}) \tag{26}$$

with m_e the electronic mass, $\mathcal{V}$ includes Coulomb interactions among the nuclei and electrons, and $\mathbf{r}_i$ and $\mathbf{R}_i$ are the coordinates of the N_e electrons and N_n nuclei, respectively.

Constructing the wave function for a system of fully interacting electrons is prohibitively difficult for more than a few tens of electrons (Kohn 1999). This presents a fundamental obstacle in solving the Schrödinger equation even for relatively simple materials. DFT proposes a solution to this dilemma by recasting the problem with the charge density $\rho_e(\mathbf{r})$ as independent variable.

The foundation of the theory is the Hohenberg-Kohn theorem (Hohenberg and Kohn 1964), which states that the ground-state charge density of a system of interacting electrons in some external potential determines this potential uniquely, i.e.,

$$\mathcal{V}\left(\mathbf{r}_1,\mathbf{r}_2,\ldots,\mathbf{r}_{N_e},\mathbf{R}_1,\mathbf{R}_2,\ldots,\mathbf{R}_{N_n}\right)\rightarrow\mathcal{V}\left[\rho_e(\mathbf{r})\right] \tag{27}$$

This allows the charge density to be used as independent variable, instead of the wave function itself, and guarantees an injective mapping between the ground state charge density and observable properties. The theorem further holds that the ground state total energy of a system is variational with respect to the electron density, i.e., the exact charge density provides the minimum possible energy for the ground state.

The theorem provides the theoretical underpinning for the Kohn-Sham approach (Kohn and Sham 1965), by which the Hamiltonian may in principle be solved exactly. The approach involves replacing the difficult interacting many body system with a non-interacting system which can be more readily solved, and then relying on the variational principle to iteratively converge on the exact solution of the interacting system. The Kohn-Sham electronic potential is then

$$\mathcal{V}^{\mathrm{KS}}\left[\rho_e(\mathbf{r})\right]=\mathcal{V}_{\mathrm{ext}}\left(\mathbf{R}_1,\mathbf{R}_2,\ldots,\mathbf{R}_{N_n}\right)+\mathcal{V}_{\mathrm{Hartree}}\left[\rho_e(\mathbf{r})\right]+\mathcal{V}_{\mathrm{xc}}\left[\rho_e(\mathbf{r})\right] \tag{28}$$

$\mathcal{V}_{\mathrm{ext}}$ being the external potential due to nuclear changes, $\mathcal{V}_{\mathrm{Hartree}}$ the Hartree potential and $\mathcal{V}_{\mathrm{xc}}$ the contribution due to electronic exchange and correlation effects.

Although DFT is exact, the functional form of $\mathcal{V}_{\mathrm{xc}}$ is not known. Recognizing this difficulty, Kohn and Sham (1965) proposed making the local density approximation (LDA), in which the exchange and correlation energy at a given point is taken as that of the homogenous electron gas with the same density, for which the solution has been parameterized (Ceperley and Alder 1980). Given its simplicity the LDA performs remarkably well for a wide variety of materials, although there are a number of instances in which it does fail. These cases are well understood, and are most often related to the presence of localized electronic states. This obstacle can in part be overcome via the more sophisticated generalized gradient approximation (GGA), which also takes charge density gradients into account when computing the exchange-correlation term.

Adding temperature

Thus far we have considered the description of the potential energy within a fully static system without any reference to the effect of kinetic energy of the atoms as expressed in the temperature. In condensed phases atoms oscillate as a result of the dynamic balance of bonding and kinetic energy; on occasion this movement is energetic enough for bonds to break, giving rise to diffusion.

Depending on the rate and complexity of such events, diffusivity can be computationally characterized by either simulating the time evolution of a representative sample at the conditions of interest, or by explicitly determining the activation parameters for the set of likely diffusion mechanisms. The first approach uses molecular dynamics, while the second combines static energy computation with vibrational frequencies obtained using lattice dynamics. More detailed descriptions of these two methods follow.

Molecular dynamics. To simulate the time evolution of a system of *N* particles requires the many body Hamiltonian to be solved, for which analytical solution is not possible. The time evolution of a system of *N* particles may be simulated numerically by integrating the system of

equations

$$\frac{\mathbf{F}_a(t)}{m_a} = \ddot{\mathbf{R}}_a \tag{29}$$

m_a being the mass of particle a, upon which the force $\mathbf{F}_a$ is obtained either as the gradient of the classical potential energy, or from the Hellmann-Feynman theorem in first-principles calculations.

The basic algorithm of molecular dynamics simulation is very simple. Given positions of the constituting particles at the current and previous time steps, $\mathbf{R}(t)$ and $\mathbf{R}(t-\Delta t)$, together with the force acting on each atom in the current time step, integrate the equations of motion (Eqn. 29) to obtain their positions at the next time step $t+\Delta t$. This is done analytically via a Taylor expansion of the position about the current time, under the constraint of interatomic forces computed from the potential energy (Verlet 1967)

$$\mathbf{R}_a(t+\Delta t) = 2\mathbf{R}_a(t) - \mathbf{R}_a(t-\Delta t) + \frac{\mathbf{F}_a(t)}{m_a}\Delta t^2 + \mathcal{O}(\Delta t^4) \tag{30}$$

More sophisticated algorithms have been developed that strive to allow larger simulation time steps, but the Verlet algorithm (Eqn. 30) remains very popular, since it is stable over long simulation periods while also having the desirable quality of time reversibility present in the equations of motion (Allen and Tildesley 1987; Frenkel and Smit 1996). Time steps used in the Verlet algorithm are normally around 0.1-1.0 fs.

Appropriate boundary conditions must be chosen in order to perform the simulation; a simple periodic boundary condition is often used. The cycle of force calculation and integration that forms the heart of the MD simulation is initiated using a reasonable choice of initial geometry, and velocities assigned according to an appropriate probability distribution (Maxwellian, Gaussian, etc.) consistent with the desired kinetic energy. Following an initial period during which the system equilibrates, it is assumed to be ergodic and time averages are computed.

Because Equation (29) is conservative, the mean total energy should remain constant during the simulation; molecular dynamics in its simplest form represents the computation of ensemble averages in the micro-canonical ensemble (constant *NVE*). Methods exist that augment the molecular dynamics algorithm to enable simulation at constant temperature (via thermostats) and constant pressure/stress (via barostats). A popular choice of thermostat, developed by Nośe (1984) and refined by Hoover (1985), maintains the mean temperature in the simulation at a specified value by extending the Lagrangian expression of Equation (29) such that the system effectively interacts with a virtual heat bath.

The Born-Oppenheimer approximation enables the time-independent DFT formulation to be applied in molecular dynamics, with the forces on the ions following via the Hellmann-Feynman theorem. This combination of DFT and molecular dynamics has been implemented at two levels of sophistication. The first is Car-Parrinello molecular dynamics (CPMD), in which the potential is obtained from a pseudo-relaxed charge density which dynamically evolves with the system (Car and Parrinello 1985). The second is Born-Oppenheimer molecular dynamics (FPMD), in which the potential is obtained from the relaxed charge density in every time step by using a finite temperature reformulation of density functional theory (Mermin 1965) in which the electronic temperature incorporated via the Fermi-Dirac distribution function (Payne et al. 1992). As a result, FPMD is more computationally intensive, but has the advantage of being more accurate and stable.

Lattice dynamics. The vibrational frequencies of the atoms at equilibrium and in the transition state (saddle point) need to be known in order to characterize solid-state diffusion. Although the potential energy surface for solids always contains some degree of anharmonicity—

especially away from equilibrium—a common approximation is to assume atomic vibrations to be small enough that the potential can be locally described as harmonic. The interaction between atom α of $\mathcal{N}$ in unit cell **m** and atom β of $\mathcal{N}$ in unit cell **n** is then

$$E^{\text{harm}}\left(\mathbf{r}(\alpha_{\mathbf{m}}),\ldots,\mathbf{r}(\beta_{\mathbf{n}}),\ldots\right) = E_0 + \frac{1}{2}\sum_{\alpha_{\mathbf{m}},\beta_{\mathbf{n}}} \Phi(\alpha_{\mathbf{m}},\beta_{\mathbf{n}})\mathbf{u}(\alpha_{\mathbf{m}})\mathbf{u}(\beta_{\mathbf{n}}) \tag{31}$$

where Φ is the force constant matrix and **u** is the displacement from equilibrium. The dynamical matrix Φ follows as the discrete Fourier transform of the force constant matrix

$$\tilde{\Phi}\left(\mathbf{q},\alpha,\beta\right) = \frac{1}{\sqrt{m_\alpha m_\beta}}\sum_{\mathbf{n}} \Phi(\alpha_{\mathbf{0}},\beta_{\mathbf{n}})\exp\left[-2\pi i\mathbf{q}\cdot(\mathbf{r}(\alpha_{\mathbf{0}})-\mathbf{r}(\beta_{\mathbf{n}}))\right] \tag{32}$$

where the summation is over all the unit cells in the crystal, and M is the molar mass. The force constant matrix can be determined by inversion of

$$\mathcal{F}_i(\alpha_{\mathbf{m}}) = -\sum_{\beta_{\mathbf{n}}} \Phi_{ij}(\alpha_{\mathbf{m}},\beta_{\mathbf{n}})\mathbf{u}_j(\beta_{\mathbf{n}}) \tag{33}$$

where the force $\mathcal{F}_i(\alpha_{\mathbf{m}})$ on atom $\alpha_{\mathbf{m}}$ resulting from displacement $\mathbf{u}(\beta_{\mathbf{n}})$ is computed through the Hellmann-Feynman theorem. The $3\mathcal{N}$ vibrational frequencies and corresponding polarization vectors follow as the eigenvalues and eigenfunctions of the dynamical matrix

$$\nu_j^2(\mathbf{q})\mathbf{e}_j(\mathbf{q}) = \tilde{\Phi}(\mathbf{q})\mathbf{e}_j(\mathbf{q}) \qquad j = 1, 3\mathcal{N} \tag{34}$$

Computation of diffusion

The nature of diffusion in melts and solids differ in timescale and geometry. At conditions well above the glass transition temperature, liquids are dynamic and isotropic, with activation energies associated with various diffusion mechanisms readily attained. Diffusion timescales are thus sufficiently short to be directly accessible by molecular dynamics simulations. As the glass transition temperature is approached, these conditions no longer apply. Diffusion in solids and glasses occurs by only a small selection of favored mechanisms, with event frequencies often in too low to be accessible by molecular dynamics simulation. The approaches followed in characterizing diffusivity thus differ fundamentally between liquids and solids.

Liquids. Liquid diffusivity is readily computed using equilibrium molecular dynamics. Two possible approaches may be followed to extract diffusivity from the phase space trajectories thus computed. The mean square displacement of each particle may be computed as a function of time, from which the relevant self-diffusivity follows by Equation (15). Alternatively the velocity autocorrelation, or mass flux correlation functions can be computed, from which the diffusivity or phenomenological coefficient matrix may be obtained through Equation (12) or (16). To determine diffusivity, the simulation time has to be about ten times longer than the relaxation time seen in the velocity autocorrelation function, which generally occurs after about a hundred time steps. Assuming the system to be ergodic, the uncertainty of the determination improves with simulation time as $t^{-1/2}$.

A concern in relatively small simulation system sizes is the effect of the periodic boundary condition on diffusivity. Due to self interaction of ions with their periodic images, diffusivities computed for small systems tend to underestimate the extrapolated infinite system size diffusivity by 5-20%. To account for this finite size effect one may perform simulations for different simulation cell sizes ℓ and extrapolate their values in the limit of $1/\ell \to 0$. By considering the diffusivity of a single sphere in a fluid continuum as a function of cell size, Yeh and Hummer (2004) and Zhang et al. (2004) showed that such an extrapolation should have the form

$$D_A^{\infty} = D_A^{N_A} + \frac{k_{\text{B}}T\xi}{6\pi\eta\ell} \tag{35}$$

where ξ is a constant (≈ 2.837297), and η is the viscosity which is best determined directly using Equation (17).

Solids. In order to describe the statistical mechanics by which diffusion in solids occurs, the enthalpies, entropies and attempt frequencies for defect/vacancy formation and migration must be computed (Eqns. 19, 22).

For a chemically pure system, the enthalpy and entropy of vacancy formation can be obtained as differences between an infinite perfect lattice and an infinite lattice containing a single vacancy (Glicksman 2000). The enthalpy of formation is then given by

$$H_A^{\mathrm{vf}} = H_A^{\mathrm{perf}} - H_A^{\mathrm{vac}} \tag{36}$$

In practice the boundary condition introduces periodic images of the vacancy, so that H_A^{vac} contains a small contribution from interaction of the vacancy with its periodic images. This interaction can be corrected for; in a cubic unit cell the correction is

$$\delta H_A^{\mathrm{vf}} = \frac{\alpha_{\mathrm{M}} z_{\mathrm{vac}}^2}{2\varepsilon_0 \ell} \tag{37}$$

where ℓ is the size of the periodic cell, z_{vac} is the charge of the vacancy, α_{M} is the Madelung constant for the particular lattice site, and ε_0 is the dielectric constant of the perfect crystal (Leslie and Gillan 1985; Brodholt 1997).

The migration enthalpy is the minimum barrier height of the migration event, and is associated with a saddle point in the potential energy surface. Although the location of the saddle point may be symmetrically evident in simple cases, this is generally not the case in more complex structured materials, where the minimum energy path often involves movement of the atom along a curved, non-symmetric path. An efficient solution may be obtained by the so-called "nudged elastic band" method (Jónsson et al. 1998), by which a trial migration path is adapted such that its barrier height is minimized. When combined with the "climbing image" scheme (Henkelman et al. 2000) the location and energy for the saddle point can be precisely found. Once the position of the saddle point is known, H_A^{vm} follows as the energy difference between the saddle point and the equilibrium position

$$H_A^{\mathrm{vm}} = E_A^{\mathrm{saddle}} - E_A^{\mathrm{equil}} \tag{38}$$

The jump frequency is similarly obtained by computing the vibrational frequencies of the equilibrium and saddle point geometries. This approach neglects anharmonicity, although anharmonic corrections have been developed (Sangster and Stoneham 1984). It is often assumed that anharmonic effects are sufficiently similar between the equilibrium position and the saddle point to effectively cancel.

SELECTED APPLICATIONS

Liquids and melts

Viscosity of the liquid outer core. The Earth's magnetic field is induced and maintained by convection in the liquid outer core, and the viscosity of liquid iron at core conditions is of key importance to understanding this process (e.g., Merrill et al. 1998). Outer core viscosities determined from geophysical observations are disparate, with values ranging between 10^{-2}-10^{10} Pa·s. In contrast, values determined using condensed matter theory suggest values to be between 10^{-4}-10^{0} Pa·s (Gans 1972; Poirier 1988; Vočadlo 2007, and references therein). These theoretical estimates are in close agreement with low pressure experimental measurements, which are very challenging above pressures of about 5 GPa (e.g., Dobson et al. 2000; Rutter et al. 2002; Terasaki et al. 2002).

Vočadlo et al. (1997), de Wijs et al. (1998) and Alfè et al. (2000) performed FPMD simulations of liquid Fe at pressures characteristic of the Earth's liquid outer core. They computed the Fe self-diffusivity using the mean square displacement slope (Eqn. 15; Fig. 2), and from this obtained the viscosity via the Stokes-Einstein relation, which has been shown to hold well for liquid metals (Dobson et al. 2000). Diffusivities thus calculated are around 5×10^{-9} m^2/s, corresponding to viscosities of 1.3×10^{-2} Pa·s, with a very similar value obtained by computing viscosity directly from the stress autocorrelation function (Eqn. 17). This value is only about ten times higher than the typical viscosities of liquid metals at ambient pressure, consistent with the suggestion of Poirier (1988) that transport properties in metals remain relatively constant along the melting curve.

It is interesting to note that these first-principles estimates are not very different from the values estimated using approximate condensed matter physics based arguments (e.g., Gans 1972). What's more, Alfè et al. (2000) compared their results for liquid structure and dynamics to values computed using a simple inverse power potential and found that such a potential gives a good representation of these physical properties in the liquid, indicating that even at the extreme pressures present in the core, Fe behaves as a simple metallic liquid. However, this result can only be derived after the fact, since there is no guarantee that the bonding behavior of Fe will remain similar at extreme pressure conditions. This is an important point to note about atomistic simulations: much insight can be gained about the atomistic behavior of systems using relatively simple stripped-down potentials, but only methods which represent the physics of bonding *directly* from first principles can be truly predictive.

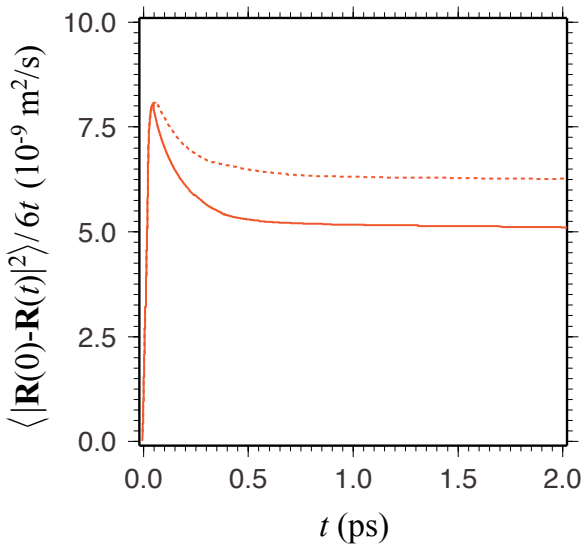

Figure 2. Diffusion coefficient for liquid Fe at 4300 K and 132 GPa, expressed as the mean square displacement $\langle r(t)\rangle$ divided by 6 × the elapsed time interval, as describe by the Einstein relation (Eqn. 15). The first-principles result (solid line) be compared to that computed using a simple inverse power potential (dotted line). The diffusivity converges to a plateaux value, the uncertainty of which is theoretically expected to decrease as $t^{-1/2}$ for longer simulation times. The initial peak is related to the movement of the atoms about their equilibrium positions, and gives an indication of its amplitude. Adapted from Alfè et al. (2000).

Melts on the MgO-SiO$_2$ join. The early thermal and chemical history of a terrestrial planet such as Earth is intimately related to processes associated with planetary-scale magma oceans. Indeed, sufficient energy sources were present for the Earth to have been entirely molten during the late stages of accretion (Urey 1955; Hanks and Anderson 1969; Ruff and Anderson 1980; Tonks and Melosh 1993). Magma ocean dynamics depend strongly on viscosity, yet values for silicate melts have only been measured up to about 15 GPa (Liebske et al. 2005). Extrapolation of these values to higher pressures is very uncertain, and depend crucially on the activation volume used in the Arrhenius relation. MgO and SiO$_2$ are the two most abundant oxide components in the mantle, and account for a dominant compositional fraction in a terrestrial magma ocean.

Due to the tremendous technical challenges associated with the laboratory investigation of silicate melts at elevated pressures (e.g., Stebbins et al. 1984; Lange and Carmichael 1987; Rivers and Carmichael 1987; Rigden et al. 1989; Reid et al. 2001; Liebske et al. 2005; Ai and Lange 2008), theoretical approaches to the study of silicate melts using empirical and semi-empirical parameterized potential sets were extensively performed during the 1980s and early 1990s (e.g., Angell et al. 1987; Kieffer and Angell 1989; Stixrude and Bukowinski 1989; Kubicki and Lasaga 1991; Cohen and Gong 1994; Matsui and Anderson 1996; Nevins and Spera 1998); these methods are now applied to very large systems for very long simulation times (e.g., Lacks et al. 2007; Adjaoud et al. 2008; Martin et al. 2009; Nevins et al. 2009). However, the speed and power of computational resources have now developed to a point where Born-Oppenheimer first-principles molecular dynamics (FPMD) can be readily performed on silicate liquids, albeit for small systems sizes, simple compositions and relatively short run times.

In a series of studies (Stixrude and Karki 2005; Karki et al. 2006, 2007, 2009; de Koker et al. 2008, 2010; Mookherjee et al. 2008; de Koker and Stixrude 2009; Stixrude et al. 2009), FPMD simulations for liquids along the MgO and SiO_2 binary were performed over the range of pressures relevant to the entire mantle. Compositions considered are MgO, Mg_5SiO_7, Mg_2SiO_4, $Mg_3Si_2O_7$, $MgSiO_3$, $MgSi_2O_5$, $MgSi_3O_7$, $MgSi_5O_{11}$ and SiO_2, as well as $12MgSiO_3 + 8H_2O$ (10 wt% water). These simulations were performed in the *NVT*-ensemble for silicate liquid systems consisting of between 72 and 112 atoms, and MgO liquid systems of 64 atoms (Stixrude and Karki 2005; Karki et al. 2006, 2007; de Koker et al. 2008, 2010). Simulations were run for at least 3000 fs, with time steps of 1 fs (0.5 fs for hydrous systems), and the first 600 fs used for equilibration. SiO_2, $MgSiO_3$, and hydrous systems were run for longer times in order to test convergence of computed diffusivities with respect to runtime (Karki et al. 2007, 2009), while system sizes of up to 400 atoms have been considered in a number of compositions to assess finite size effects.

Self-diffusivities for these systems were determined from the mean squared displacement slope (Eqn. 15), and show a consistent trend of $D_{Si} < D_O < D_{Mg}$ along the binary (Fig. 3). Self-diffusivities for all species are enhanced by about a factor of four in the hydrous melt, with the H value higher than those of the other species by almost an order of magnitude. Self-diffusivities for all species are lower at elevated pressures, although for H the decrease is significantly smaller. At low temperatures D_{Si}, and to a lesser extent D_O, initially increases upon compression for $X_{SiO_2>0.5}$. Analysis of finite size effects suggests that computed diffusivities underestimate values extrapolated to infinite system sizes by about 10-20%.

With the exception of the low *P-T* behavior, self-diffusivities are well represented by an Arrhenian relation

$$D_A(P,T) = D_A^0 \exp\left[-\frac{E_A^a + PV_A^a}{k_B T}\right] \tag{39}$$

E_A^a and V_A^a being the activation energy and volume of species A, with D_A^0 the limiting diffusivity as $T \to \infty$; the low *P-T* increases in self-diffusivity imply activation volumes that are locally negative.

In the dry melt compositions, activation energies for Mg is consistently the lowest and for Si the highest. Values decrease notably with SiO_2 content, flattening out for $X_{SiO_2} < 0.4$ (Fig. 4). Activation energy values for Si and O are very similar at high SiO_2 concentrations, but diverge as concentration decreases. Relationships in Arrhenian parameters between Mg, Si and O exhibited in the dry melt are also seen in the hydrous melt. Activation volumes and limiting diffusivities are very similar to the anhydrous melts, but activation energy of the hydrous melt is notably depressed.

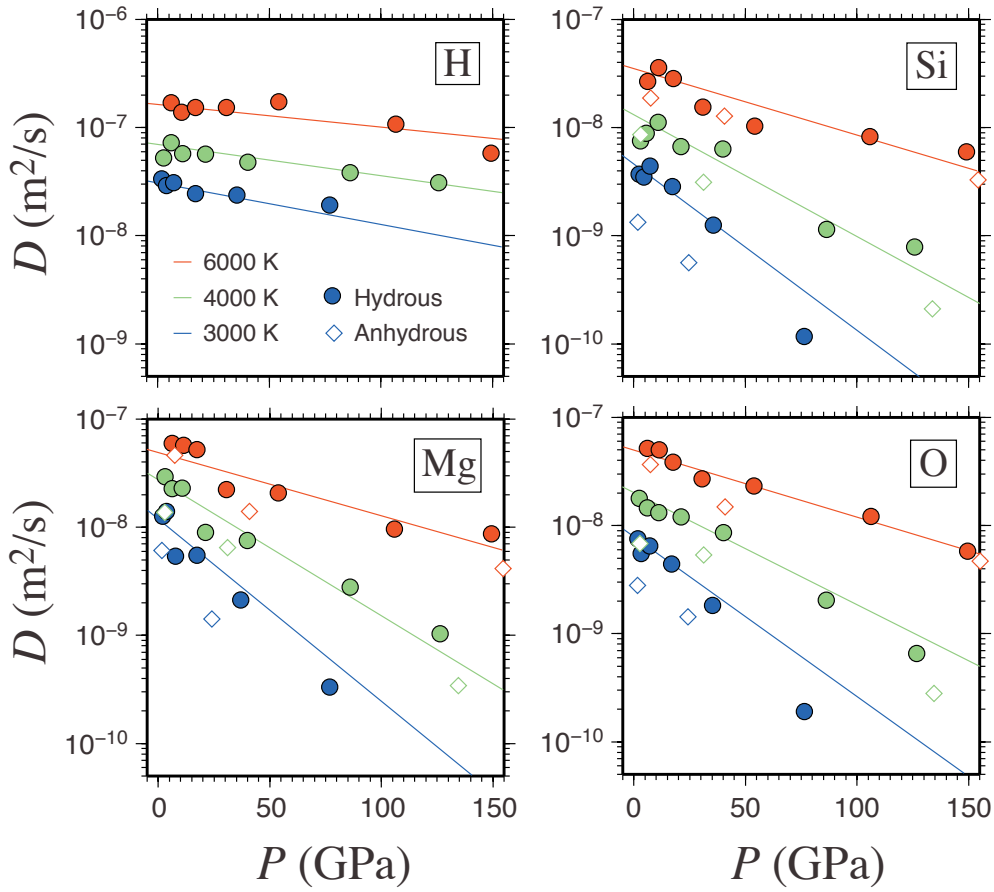

Figure 3. Self-diffusivities in hydrated $MgSiO_3$ melt with 10 wt% H_2O, with lines indicating the Arrhenius fit. Data from Karki et al. (2009) and Mookherjee et al. (2008).

The relative mobilities of various species can be understood in the context of differences in the character of bonding and changes in liquid structure with SiO_2 content. The most notable structural trend is the change in oxygen speciation, as expressed by the oxygen coordination with respect to silicon ($Z_{O\text{-}Si}$). At all degrees of compression the $Z_{O\text{-}Si}$ distribution shifts to lower values as SiO_2 content decreases, with polyhedral species ($Z_{O\text{-}Si} \geq 2$) especially rare for $X_{SiO_2} < 0.4$ (de Koker et al. 2010). Therefore, at temperatures close to melting, self-diffusion occurs more readily in the absence of a highly polymerized framework, while the presence of free oxygen ($Z_{O\text{-}Si} = 0$) in addition to non-bridging oxygen ($Z_{O\text{-}Si} = 1$) does not have a notable effect on diffusivity. Interestingly, analysis of bond lifetimes reveal that free oxygen is notably longer lived than more highly coordinated oxygen species (de Koker et al. 2008).

Because diffusion occurs through continuous breaking and forming of old and new bonds, one cannot describe self-diffusion of a given species without also invoking mechanisms by which other species migrate. Visualization and analysis of liquid dynamics indicate that diffusion mechanisms can be well described in terms of increases and decreases in coordination. One pair of events would be[2]

$$O_F + {}_{[Z]}Si^{Q} \rightarrow O_N + {}_{[Z+1]}Si^{Q} \tag{40}$$

followed by

2 We describe the local structure about Si atoms as ${}_{[Z]}Si^{Q}$, with [Z] the coordination number and Q the number of bridging oxygens; O speciation is denoted by O_F for free oxygen, O_N for non-bridging oxygen and O_B for bridging oxygen.

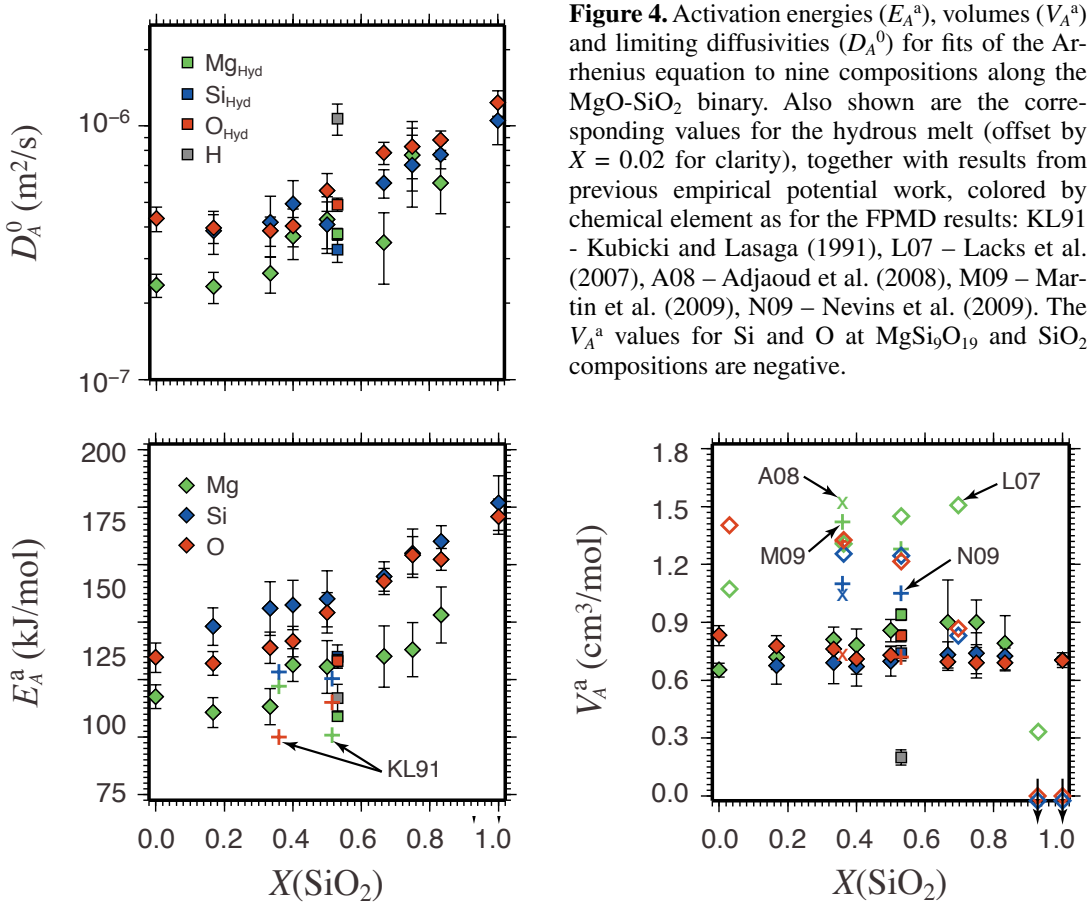

Figure 4. Activation energies (E_A^a), volumes (V_A^a) and limiting diffusivities (D_A^0) for fits of the Arrhenius equation to nine compositions along the MgO-SiO_2 binary. Also shown are the corresponding values for the hydrous melt (offset by $X = 0.02$ for clarity), together with results from previous empirical potential work, colored by chemical element as for the FPMD results: KL91 - Kubicki and Lasaga (1991), L07 – Lacks et al. (2007), A08 – Adjaoud et al. (2008), M09 – Martin et al. (2009), N09 – Nevins et al. (2009). The V_A^a values for Si and O at $MgSi_9O_{19}$ and SiO_2 compositions are negative.

$$O_B^* + {}_{[Z+1]}Si^Q \rightarrow O_N^* + {}_{[Z]}Si^{Q-1} \tag{41}$$

with * denoting a distinct oxygen atom. Reversed event pairs are also observed,

$$O_N + {}_{[Z]}Si^Q \rightarrow O_F + {}_{[Z-1]}Si^Q \tag{42}$$

followed by

$$O_N^* + {}_{[Z-1]}Si^Q \rightarrow O_B^{**} + {}_{[Z]}Si^{Q+1} \tag{43}$$

Over time, a single atom will traverse large distances by repeated working of a combination of these types of events. However, free oxygen is unique in this scheme: it can only undergo increases in coordination, and thus have only half the general diffusion pathways available to it. This may explain its prolonged mean lifetime, as well as the observation that activation energies level off at low SiO_2 concentrations.

Higher diffusivities in the hydrated melt can also be well understood in terms of liquid structure. With the presence of additional oxygen, the average oxygen-silicon coordination is decreased, resulting in a less polymerized liquid in which hydrogen binds especially to the free- and non-bridging oxygen species (Karki et al. 2009). As seen in the dry melt, a decrease in bridging oxygen results in decreased activation energy for all species present in the melt, as non-bridging and free oxygens more readily serve as hosts for transition states associated with the various diffusion mechanisms. Indeed Karki et al. (2009) identified two main hydrogen diffusion mechanisms. The first involves hydrogen atoms forming and breaking bonds with polyhedral oxygen ($Z_{O\text{-}Si} \geq 1$), thus always staying directly associated with the silica framework via H-O-Si bonds (Fig. 5). The second involves the special case when a hydrogen atom binds

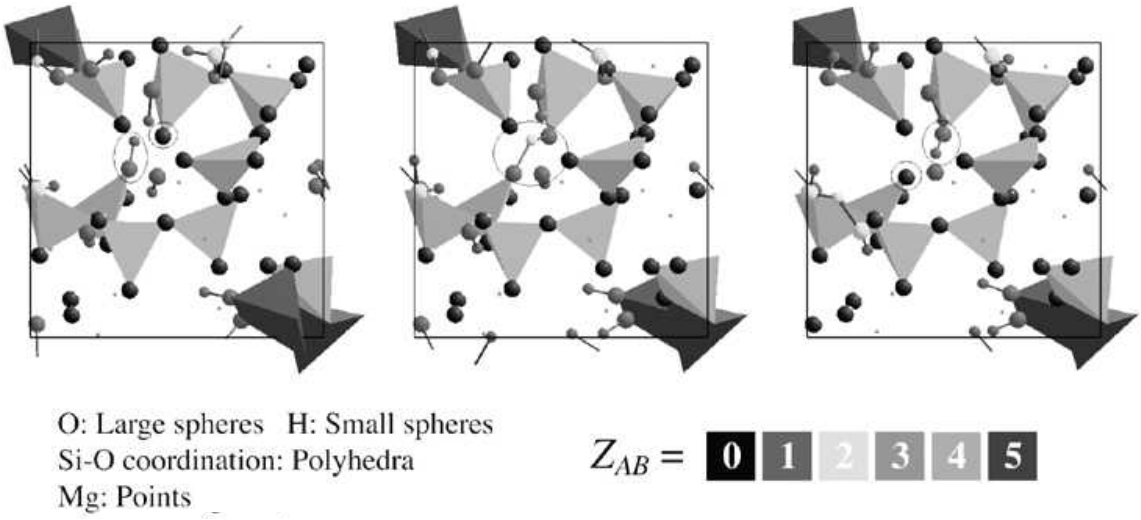

Figure 5. Snapshots of FPMD simulations of hydrous $MgSiO_3$ melts, illustrating the transfer of a hydrogen atom between two silica polyhedra, as indicated by the circles. From Karki et al. (2009). [Used by permission of Springer, from Karki et al. (2009), *Physics and Chemistry of Minerals*, Vol. 37, p. 103-117.]

to a free oxygen ($Z_{O\text{-}Si} = 0$), to form hydroxyl species that are unusually long lived for similar reasons to those described for free oxygen.

The high self-diffusivity of H suggests that hydrated melts could have high conductivity, which would make them geophysically detectable in the upper mantle by magnetotelluric sounding. Using the Nernst-Einstein relation, Mookherjee et al. (2008) computed that hydrated melt should have a conductivity of 59 c/10 S/m, so that a 20 km thick layer of 5 vol% partial mantle melt containing 3 wt% water will have a conductivity of 18 S/m, and would be geophysically observable.

Hydrothermal fluids and aqueous solutions. Hydrothermal fluids are responsible for many rare and unusual mineralogical deposits. They accumulate, transport, fractionate and concentrate incompatible trace elements from the crust and upper mantle, and are the source for many ore deposits of noble metals and pegmatitic minerals. Ascending hydrothermal fluids associated with subduction processes are very reducing, commonly at temperatures of around 400-1100 K (e.g., Manning 2004), and dissolve large concentrations of silica while also scavenging trace incompatible elements from the country rock. This dissolved load is deposited at shallow depths as the fluid cools, decompresses, and becomes oxidized.

Almost all theoretical studies of water have focused on ambient conditions. This is in part because water at these conditions is of central importance to many fields of chemistry, but also because water is in fact a rather unusual substance, with bonding characteristics not easily captured with existing first-principles techniques (Silvestrelli and Parrinello 1999; Grossman et al. 2004). It is well known that the structure of pure water is disrupted by a solute; dissolved ions are surrounded by water molecules arranged to form multiple solvation shells. The structure of these solvation shells has been studied in detail both experimentally as well theoretically (e.g., Ohtaki and Radnai 1993; Bakker 2008). The characteristic residence time of a water molecule in the first solvation shell is a key parameter in models describing the structural dynamics by which solute diffusion in aqueous solutions takes place. However, this parameter is difficult to constrain uniquely from experiment, and molecular dynamics simulations have been indispensable in elucidating general trends between diffusivity and parameters describing the first solvation shell.

Although a number of theoretical studies have considered aqueous silica solutions (Cheng

et al. 2002; Tossel 2005), the diffusive properties of dissolved silica have only been partly addressed. Doltsinis et al. (2007) considered the diffusivities of various candidate molecular species that silica may form in aqueous solution at ambient pressure using Car-Parrinello molecular dynamics (CPMD). Their results indicate that the diffusivity of silica complexes (e.g., SiO_4H_4), which diffuse as single structural units at these temperatures, decreases if the size of the silica complex is increased (e.g., to $Si_2O_7H_6$ or $Si_3O_{10}H_8$). This result can be understood in terms of the Stokes-Einstein relation: increasing the size of the silica complex results in a large effective diameter of the solute, and therefore a decrease in diffusivity.

Although our understanding of chemical diffusion has progressed greatly since the experiments of Graham (1833) and Fick (1855), saline aqueous solutions continue to form a cornerstone in investigating the mechanisms and interesting effects associated with the phenomenon. We will highlight two examples, the first relating to mass-dependent diffusion, and the second to the characterization of cross-diffusivity and the full diffusion matrix.

While differences in nuclear mass among isotopes have a negligible effect on bonding, differences in inertia can be sufficient to bring about isotopic fractionation by diffusion. Examples include the correlated enrichment in heavy isotopes of Mg and Si within Ca-Al rich inclusions (CAI's) found in meteorites (Richter et al. 2007), major element isotope fractionation in melts (Richter et al. 2008, 2009), and fractionation of ionic species in water (Richter et al. 2006).

For a dilute gas, kinetic theory of diffusion (e.g., McQuarrie 1984) predicts that the ratio of diffusion coefficients D_A and D_B of two species of respective molar mass values m_A and m_B is given by

$$\frac{D_A}{D_B} = \left(\frac{m_B}{m_A} \right)^{\beta} \tag{44}$$

with $\beta = 0.5$. From experimental measurements for aqueous solutions (e.g., Richter et al. 2006), the value of β for diffusion in liquid water is known to be notably less than 0.5, yet still large enough for mass dependent isotope fractionation to occur. Molecular dynamics simulations of solute diffusion in liquid water have helped elucidate the mechanisms by which such fractionation takes place (Nuevo et al. 1995; Willeke 2003; Bourg and Sposito 2007, 2008). Indeed, numerical simulation is especially powerful for investigating mass dependent diffusion because one can access a large range of hypothetical nuclear mass values that do not occur in nature, greatly improving the accuracy with which mass dependent fractionation is constrained.

Using a standard description of the water molecule (Berendsen et al. 1987), together with very simple Lennard-Jones type potential representations of the interactions among molecules and solute ions, Bourg and Sposito (2007, 2008) considered the mass dependent fractionation in water of Li^+, Mg^{+2}, Cl^-, He, Ne, Ar and also Xe. The simplicity of the potential allows for simulation over very long runtimes (8 ns) with relatively large system sizes (550-1000 atoms). The results of Bourg and Sposito (2007, 2008) show excellent agreement with the available experimental data for Li, Mg, and Cl (Fig. 6) and further predict strong mass dependent fractionation of noble gasses in water, for which no experimental data is available yet.

Cross-diffusivities are rather challenging to determine from experiment, so that various approximate treatments are used to describe the effect (e.g., Zhang 2008, 2010). A statistical mechanical description of multicomponent diffusion useful for computational studies was only recently derived (Zhou and Miller 1996; Wheeler and Newton 2004). To implement and test this set of equations, Wheeler and Newton (2004) used molecular dynamics simulations very similar to those of Bourg and Sposito (2007) to compute the full diffusion matrix for aqueous solutions of NaCl and KCl. Results show very good agreement with experimental measurements at room temperature (Fig. 7), especially in the light of the relative simplicity of the potentials used.

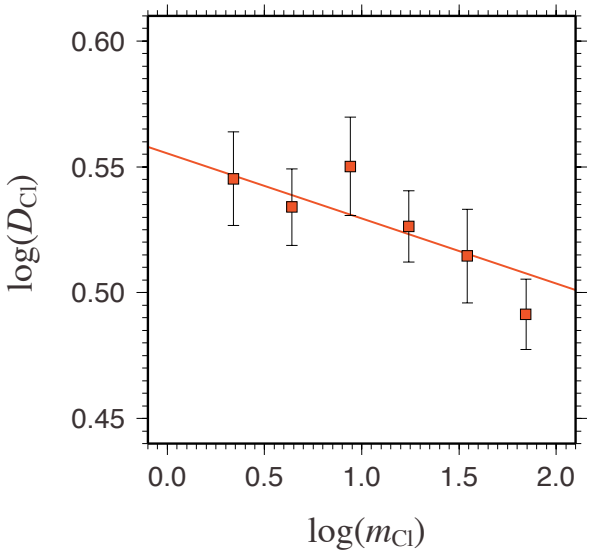

Figure 6. Determination of the mass dependence of diffusivities using MD can be done readily by accessing very large and very small hypothetical molar masses not available to experimental measurement. The solid line represents the expected trend from experimental data of Richter et al. (2006). Diffusivities are in 10^{-9} m^2/s. Adapted from Bourg and Sposito (2007).

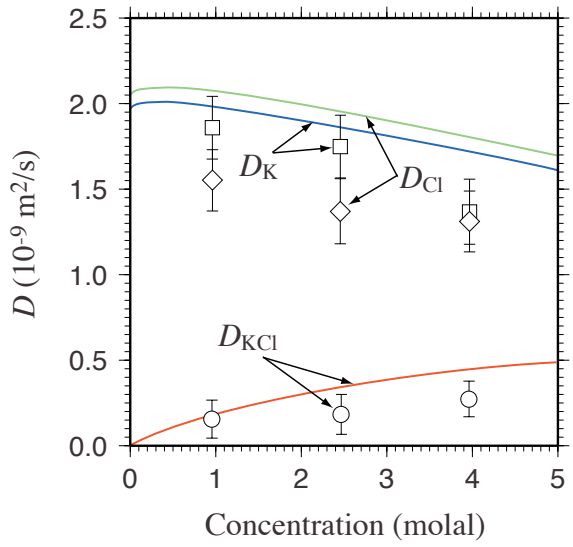

Figure 7. Diagonal and off-diagonal components for the diffusion matrix of KCl aqueous solutions computed using classical molecular dynamics simulations, compared to a compilation of experimental data. Adapted from Wheeler and Newton (2004).

Solids

Deep mantle phases. An issue of great importance to deep Earth science concerns the rheology of the mantle. Modeling of geoid, post-glacial rebound, and tectonic plate velocity data, suggests the viscosity of the lower mantle to vary between 10^{21}-10^{23} Pa·s (Richards and Hager 1984; Hager et al. 1985; Mitrovica and Forte 2004), and also reveal the presence of lateral variations in viscosity at the core-mantle boundary (Čadek and Fleitout 2006; Tosi et al. 2009). However, the mineralogical underpinnings of these observations are not well understood.

Based on a variety of geodynamic and mineralogical arguments, the dominant mechanism of solid-state flow in the lower mantle is believed to be diffusion creep (e.g., Karato et al. 1995). A thorough understanding of solid-state diffusion in the lower mantle is therefore the key to understanding the rheology of the lower mantle in an atomistic context.

As is often the case in theoretical work, the early studies have focussed mostly on MgO periclase because of its simple structure and computational economy. Initial studies applied relatively simple parameterized potentials at ambient pressures (Sangster and Stoneham 1984; Vočadlo et al. 1995), with more recent work using *ab initio* and first-principles methods to consider diffusion at lower mantle pressures (Ita and Cohen 1998; Karki and Kanduja

2006; Ammann et al. 2009b, 2010). These studies found good agreement with the available experimental data, and highlighted the fact that in mantle minerals the role of minor and trace elements in vacancy formation (extrinsic) dominates over formation of simple Schottky defects in a pure system (intrinsic). Therefore vacancy concentrations can be obtained from measured impurity concentrations, rather than by calculations of the free energy of vacancy formation.

Early studies of perovskite notably overestimated the experimental Si activation energy as a result of incorrect identification of saddle point locations (Wright and Price 1993; Karki and Kanduja 2007). Ammann et al. (2009b) identified the possible diffusion paths for self-diffusion of Mg, Si and O, and located the relevant saddle points by applying the climbing-image nudged elastic band method. After characterizing the migration enthalpy, entropy and vibrational frequencies, they obtained vacancy self-diffusivities for each of these species in the various crystallographic directions. They found that Mg and O self-diffusion occur respectively as simple jumps into vacancies on Mg and O lattice sites, while Si diffuses most readily via a six jump cycle (Fig. 1). After further analysis they found these cycles to break 1-20% of the time due to electrostatic repulsion, and speculate that the effect can be reduced by the presence of proton defects (i.e., H^+ ions).

Building on their earlier results, Ammann et al. (2010) characterized diffusivity in $MgSiO_3$ post-perovskite. Diffusivities for Si and Mg were found to be extremely anisotropic. Interestingly, this anisotropy is not directly related to the layered structure but rather to the fact that, because Si-O octahedra share edges in the [100] direction and corners in the [001] direction, a series of channels exist in the [100] direction along which migration enthalpies are low. Diffusion of both Si and Mg in the [010] direction (across layers) was found to occur by six jump cycles. Self-diffusivities of Mg, Si and O in periclase, perovskite and post-perovskite are shown in Figure 8.

When combined with experimental estimates of extrinsic vacancy concentration values, the low pressure periclase and perovskite diffusivities of Ammann et al. (2009a,b) show excellent agreement with measurements. Mantle viscosity values computed from their results along the mantle geotherm further show close agreement with the profile derived from post-glacial rebound and the geoid.

He in zircon: thermochronometry. The ability to model the denudation history of tectonically active regions using thermochronometry has revolutionized the fields of geomorphology and tectonics, providing a deeper understanding of the the coupling between the evolution of the Earth's surface, interior and atmosphere (e.g., Parrish 1985; Farley et al. 2001; Hodges 2003; Ehlers 2005; Ehlers and Poulsen 2009). The premise for thermochronometry is the insight that at temperatures below some characteristic value (closure temperature) diffusion in minerals is so slow that that noble gas daughter isotopes of radioactive decay processes are retained in crystal grains and fission tracks do not anneal (Dodson 1973). Measurements of daughter isotope- or fission track retention in a mineral grain can therefore provide a thermal age for its host rock, essentially dating the time that has passed since the rock was last at the closure temperature.

Experimental measurements of He diffusivity in zircon ($ZrSiO_4$) indicate a closure temperature of 450 K for the zircon (U-Th)/He thermochronometer (Reiners et al. 2004). However, these measurements also suggest that He diffusion in zircon is not strictly Arrhenian below about 650 K, and assume diffusivity in zircon to be isotropic. Zircon is tetragonal with an open structure forming a series of channels in the [100], [101], and [001] directions, along which He could possibly migrate with relative ease.

To better characterize He diffusion in zircon, Reich et al. (2007) determined the migration enthalpy of He diffusion in zircon as a function of crystallographic direction, and performed molecular dynamics simulations to characterize the temperature dependent behavior of

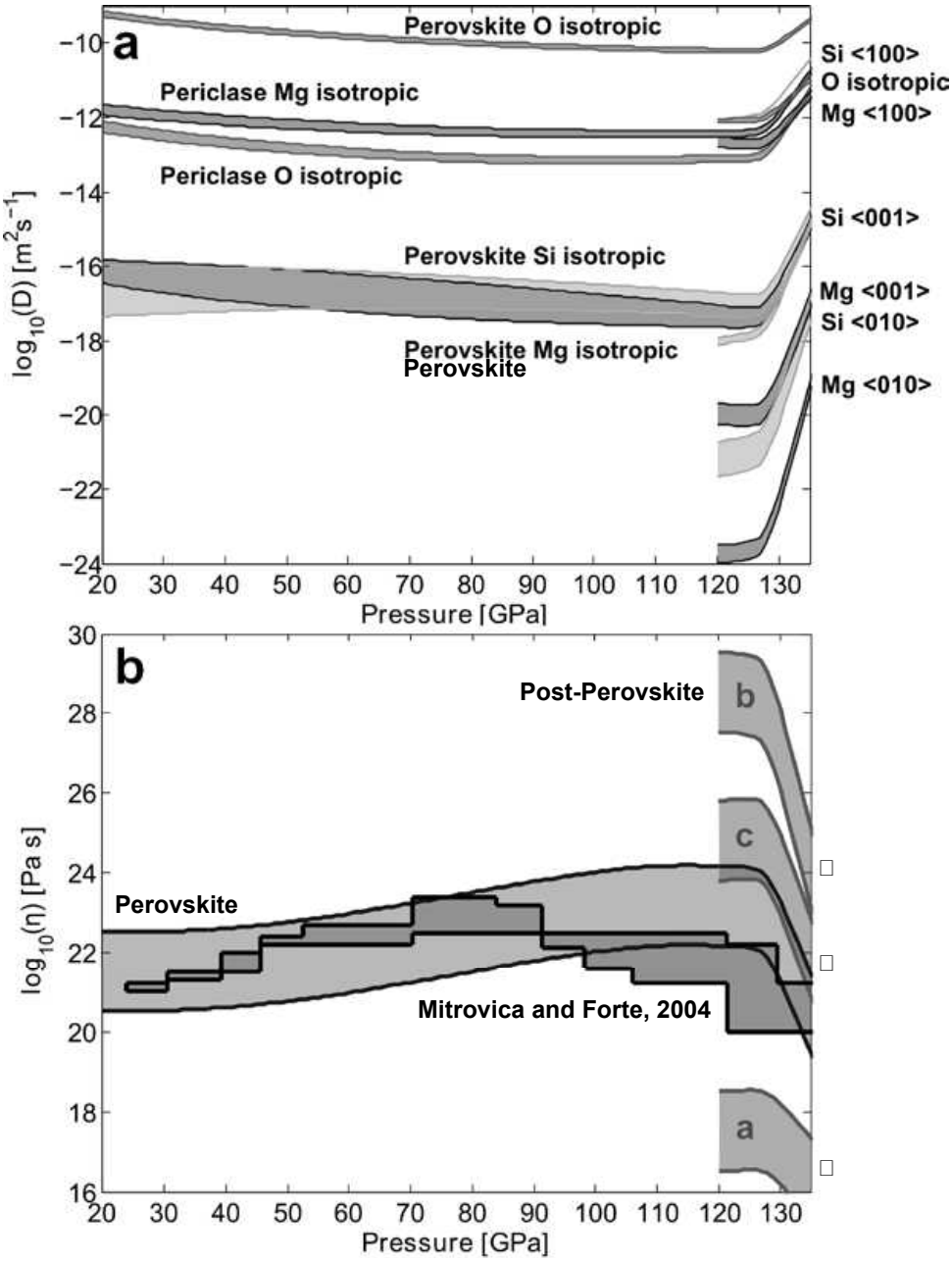

Figure 8. a) Vacancy diffusion coefficients in MgO periclase, $MgSiO_3$ perovskite and $MgSiO_3$ post-perovskite computed along a geotherm. Upper bounds – LDA; Lower bounds – GGA. b) Associated viscosity profile for the mantle, computed assuming diffusion creep, compared to estimates of Mitrovica and Forte (2004) from inverse modeling of geophysical data. Post-perovskite values are end-member viscosities along crystallographic axes. [Reprinted from Macmillan Publishers Ltd: *Nature*, Ammann et al. (2010). doi:10.1038/nature09052]

anisotropy. Their calculations employed a standard combination of the Born-Mayer and Coulomb potential, for which they constrained the parameters using experimental data for zircon, and quantum mechanical calculations of the energies of He-Zr, He-Si and He-O interaction pairs. They found the migration enthalpy for He diffusion to be smallest in the [001] direction (13.4 kJ/mol), followed by the [100] and [101] directions (44.8 kJ/mol and 101.7 kJ/mol, respectively). Their molecular dynamics simulations revealed that at room temperature He migrates only along the channels in the [001] direction, while hops in the [100] direction to neighboring [001] channels become increasingly common at temperatures of around 600

K; at temperatures above 850 K He moved freely in both the [100] and [001] directions. This change in the extent of anisotropic diffusion with temperature may explain the apparent non-Arrhenian behavior seen in the experimental measurements, and highlights the need to also consider anisotropy when interpreting zircon (U-Th)/He thermochronometry data.

A VIEW TO THE FUTURE

Looking back 50 years to the first atomistic simulation studies, the degree to which the state of the art has advanced is staggering, and one is left somewhat daunted by the prospect of what will be possible 50 years into the future. More perspective can perhaps be gained by looking back only 15 years to when Born-Oppenheimer FPMD started to be applied to a broad variety of problems. These early calculations generally involved system sizes of around 60 atoms and run times of about 2000 time steps, yet required very large computational resources to perform. Since then, accessible system sizes and run times have increased by almost a factor of 20, but more importantly, the computational resources required to perform FPMD for a modest system of around 100 atoms and run times on the order of 5000 time steps have become small enough for simulations to be readily performed in parallel on 16 processors in 24 hours.

For system sizes of around 100 atoms, the uncertainty in diffusivities determined with FPMD is on the order of 5-10%. Theoretically, the uncertainty should decrease with simulation run time as $t_{run}^{-1/2}$. Run durations of around 4 times longer are therefore required to reduce uncertainties by a factor of two. In the context of system size, a factor two reduction in the magnitude due to the finite size of the simulation system would require system sizes 8 times larger (Eqn. 35).

Density functional theory based codes generally scale as n_e^3 of the number of electrons treated in the system. Projections of system sizes accessible to these methods place the largest systems in the order of 10,000 atoms by the year 2020, while the "average" FPMD run projects to around 1000 atoms (Head-Gordon and Artacho 2008). However, over the last 10 years codes that scale more efficiently with n_e have been under development, and are already reaching sizes on the order of 10,000 atoms. As these methods improve, accurate and robust treatment of very large systems with complex chemistry at colder temperatures (close to or below melting) would become viable. An exciting prospect of such developments for geological systems would be the ability to directly model processes in natural melts.

New developments in the theory of electronic structure calculations can also be expected, with the treatment of highly localized states and strongly correlated systems coming to mind as two promising improvements. This would make the treatment of transition metals more reliable, and open numerous new avenues to explore the mineral physics and geochemistry of systems where these elements play a key role.

ACKNOWLEDGMENTS

This work was made possible by support from the European Commission under contract MRTN-CT-2006-035957 to NDK. We are grateful to Michael Ammann for sharing his draft manuscripts, and to Youxue Zang, James van Orman and an anonymous reviewer for insightful comments.

REFERENCES

Adjaoud O, Steinle-Neumann G, Jahn S (2008) Mg_2SiO_4 liquid under high pressure from molecular dynamics. Chem Geol 256:185-192

Ai Y, Lange RA (2008) The Compressibility of CaO-MgO-Al_2O_3-SiO_2 liquids from new acoustic velocity measurements: reevaluation of the equation of state of $CaMgSi_2O_6$-$CaAl_2SiO_8$ liquids to 25 GPa. J Geoophys Res 113:B04203

Alder BJ, Wainwright TE (1957) Phase transition for a hard sphere system. J Chem Phys 27:1208-1209

Alfè D, Kresse G, Gillan (2000) Structure and dynamics of liquid iron under Earth's core conditions. Phys Rev B 61:132-142

Allen MP, Tildesley DJ (1987) Computer Simulation of Liquids. 1st Edition. Oxford University Press, Oxford,

Ammann MW, Brodholt JP, Dobson DP (2009a) DFT study of migration enthalpies in $MgSiO_3$ perovskite. Phys Chem Miner 36:151-158

Ammann MW, Brodholt JP, Dobson DP (2009b) Simulating diffusion. Rev Mineral Geochem 71:201-224

Ammann MW, Brodholt JP, Wookey J, Dobson DP (2010) First-principles constraints on diffusion in lower-mantle minerals and a weak D″ layer. Nature 465:462-465, doi:10.1038/nature09052

Angell CA, Cheeseman PA, Kadiyala RR (1987) Diffusivity and thermodynamic properties of diopside and jadeite melts by computer simulations. Chem Geol 62:83-92

Bakker HJ (2008) Structural dynamics of aqueous salt solutions. Chem Rev 108:1456-1473

Berendsen HJC, Grigera JR, Straatsma TP (1987) The missing term in effective pair potentials. J Phys Chem 91:6269-6271

Birch F (1952) Elasticity and constitution of the Earth's interior. J Geoophys Res 57:227-286

Borg RJ, Dienes GJ (1988) Solid State Diffusion. Academic Press, Boston

Bourg IC, Sposito G (2007) Molecular dynamics simulations of kinetic isotope fractionation during the diffusion of ionic species in liquid water. Geochim Cosmochim Acta 71:5583-5589

Bourg IC, Sposito G (2008) Isotopic fractionation of noble gases by diffusion in liquid water: Molecular dynamics simulations and hydrologic applications. Geochim Cosmochim Acta 72:2237-2247

Brodholt J (1997) *Ab initio* calculations on point defects in forsterite (Mg_2SiO_4) and implications for diffusion and creep. Am Mineral 82:1049-1053

Burton JJ (1972) Vacancy-formation entropy in crystals. Phys Rev B 5:2948-2957

Čadek O, Fleitout L (2006) Effect of lateral viscosity variations in the core-mantle boundary region on predictions of the long-wavelength geoid. Studia Geophys Geod 50:217-232

Callen HB (1985) Thermodynamics and an Introduction to Thermostatistics. 2nd Edition. John Wiley & Sons, New York

Callen HB, Welton TA (1951) Irreversibility and generalized noise. Phys Rev 83:34-40

Car R, Parrinello M (1985) Unified approach to molecular dynamics and density-functional theory. Phys Rev Lett 55:2471-2474

Ceperley DM, Alder BJ (1980) Ground-state of the electron-gas by a stochastic method. Phys Rev Lett 45:566-569

Chandrasekhar S (1943) Stochastic problems in physics and astronomy. Rev Mod Phys 15:1-89

Cheng HP, Barnett RN, Landman U (2002) Structure, collective hydrogen transfer, and formation of $Si(OH)_4$ in SiO_2-$(H_2O)_n$ clusters. J Chem Phys 116:9300-9304

Cohen RE, Gong Z (1994) Melting and melt structure of MgO at high pressures. Phys Rev B 50:12301-12311

Crank J (1975) The Mathematics of Diffusion. 2nd Edition. Oxford University Press, Oxford

de Groot SR, Mazur P (1969) Non-Equilibrium Thermodynamics. North-Holland, Amsterdam

de Koker N, Karki BB, Stixrude L (2010) Mixing, structure and freezing of MgO-SiO_2 liquids in Earth's lower mantle. (in prep)

de Koker N, Stixrude L (2009) Self-consistent thermodynamic description of silicate liquids, with application to shock melting of MgO periclase and $MgSiO_3$ perovskite. Geophys J Int 178:162-179

de Koker N, Stixrude L, Karki BB (2008) Thermodynamics, structure, dynamics, and freezing of Mg_2SiO_4 liquid at high pressure. Geochim Cosmochim Acta 72:1427-1441, doi:10.1016/j.gca.2007.12.019

de Wijs GN, Kresse G, Vočadlo L, Dobson D, Alfè D, Gillan MJ, Price GD (1998) The viscosity of liquid iron at the physical conditions of the Earth's core. Nature 392:805-807

Dobson DP, Crichton WA, Vočadlo L, Jones AP, Wang Y, Uchida T, Rivers M, Sutton S, Brodholt J (2000) *In situ* measurement of viscosity of liquids in the Fe-FeS system at high pressures and temperatures. Am Mineral 85:1838-1842

Dodson MH (1973) Closure temperature in cooling geochronological and petrological systems. Contrib Mineral Petrol 40:259-274

Doltsinis NL, Burchard M, Maresch WV, Boese AD, Fockenberg T (2007) Ab initio molecular dynamics study of dissolved SiO_2 in supercritical water. J Theor Comput Chem 6:49-62

Ehlers TA (2005) Crustal thermal processes and the interpretation of thermochronometer data. Rev Mineral Geochem 58:315-350

Ehlers TA, Poulsen CJ (2009) Influence of Andean uplift on climate and paleoaltimetry estimates. Earth Planet Sci Lett 281:238-248

Einstein A (1905) Über die von der Molekularkinetischen Theorie der Wärme geforderte Bewegung von in ruhenden Flüssigkeiten suspendierten Teilchen. Annal Phys 322:549-560

Elcock EW (1959) Vacancy diffusion in ordered alloys. Proc Physical Soc 73:250-264
Eyring H (1936) Viscosity, plasticity and diffusion as examples of absolute reaction rates. J Chem Phys 4:283-291
Farley KA, Rusmore ME, Bogue SW (2001) Post-10 Ma uplift and exhumation of the northern coast mountains, British Columbia. Geology 29:99-102
Fick A (1855) Über Diffusion. Poggendorff's Annalen der Physik und Chemie 94:59-86
Fourier J (1822) Théorie Analytique de la Chaleur. Firmin Didot, Paris
Frenkel D, Smit B (1996) Understanding Molecular Simulation: From Algorithms to Applications. 1st Edition. Academic Press, San Diego
Gale JD (1998) GULP - a computer program for the symmetry adapted simulation of solids. J Chem Soc Faraday Trans 93:629-637
Gale JD (2001) Simulating the Crystal Structures and Properties of Ionic Materials from Interatomic Potentials. Rev Mineral Geochem 42:37-62
Gans RF (1972) Viscosity of the Earth's core. J Geoophys Res 77:360-366
Gillan MJ, Jacobs PWM (1983) Entropy of a point defect in an ionic crystal. Phys Rev B 28:759-777
Glicksman ME (2000) Diffusion in Solids: Field Theory, Solid-State Principles, and Applications. 1st Edition. John Wiley and Sons, New York
Graham T (1833) Researches on the arseniates, phosphates, and modifications of phosphoric acid. Philos Trans Royal Soc 123:253-284
Green MS (1952) Markoff random processes and the statistical mechanics of time-dependent phenomena. J Chem Phys 20:1281-1295
Grossman JC, Schwelger E, Draeger EW, Gygi F, Galli G (2004) Towards an assessment of the accuracy of density functional theory for the first principles simulations of water. J Chem Phys 120:300-311
Hager B, Clayton R, Richards M, Comer R, Dziewonski A (1985) Lower mantle heterogeneity, dynamic topography and the geoid. Nature 313:541-545
Hanks TC, Anderson DL (1969) The early thermal history of the Earth. Phys Earth Planet Inter 2:19-29
Hansen JP, McDonald IR (2006) Theory of Simple Liquids. 3rd Edition. Academic Press, London
Head-Gordon M, Artacho E (2008) Chemistry on the computer. Physics Today 61:58-63
Henkelman G, Uberuaga BP, Jónsson H (2000) A climbing image nudged elastic band method for finding saddle points and minimum energy paths. J Chem Phys 113:9901-9904
Hodges KV (2003) Geochronology and thermochronology in orogenic systems. *In:* Treatise of Geochemistry, Volume 3: The Crust. Rudnick RL (ed) Elsevier, p 263-292
Hohenberg P, Kohn W (1964) Inhomogeneous electron gas. Phys Rev 136:864-871
Hoover WG (1985) Canonical dynamics: equilibrium phase-space distributions. Phys Rev A 31:1695-1697
Ita J, Cohen RE (1998) Diffusion in MgO at high pressure: implications for lower mantle rheology. Geophys Res Lett 25:1095-1098
Jónsson H, Mills G, Jacobsen KW (1998) Nudged elastic band method for finding minimum energy paths of transitions. *In:* Classical and Quantum Dynamics in Condensed Phase Simulations. BJ Berne, G Ciccotti, DF Coker (eds), World Scientific, Singapore, p 385-404
Karato SI, Zhang S, Wenk H-R (1995) Superplasticity in Earth's lower mantle: evidence from seismic anisotropy and rock physics. Science 270:458-461
Karki BB, Bhattarai D, Mookherjee M, Stixrude L (2009) Visualization-based analysis of structural and dynamical properties of simulated hydrous silicate melt. Phys Chem Miner 37:103-117
Karki BB, Bhattarai D, Stixrude L (2006) First principles calculations of the structural, dynamical and electronic properties of liquid MgO. Phys Rev B 73:174208
Karki BB, Bhattarai D, Stixrude L (2007) First-principles simulations of liquid silica: Structural and dynamical behavior at high pressure. Phys Rev B 76:104205
Karki BB, Kanduja G (2006) Vacancy defects in MgO at high pressure. Am Mineral 91:511-516
Karki BB, Kanduja G (2007) A computational study of ionic vacancies and diffusion in $MgSiO_3$ perovskite and post-perovskite. Earth Planet Sci Lett 260:201-211
Kieffer J, Angell CA (1989) Structural incompatibilities and liquid-liquid phase separation in molten binary silicates: A computer simulation. J Chem Phys 90:4982-4991
Knopoff L, Uffen RJ (1954) The densities of compounds at high pressures and the state of the Earth's interior. J Geoophys Res 59:471-484
Kohn W (1999) Nobel lecture: electronic structure of matter - wave functions and density functionals. Rev Mod Phys 71:1253-1266
Kohn W, Sham LJ (1965) Self-consistent equations including exchange and correlation effects. Phys Rev 140:1133
Kubicki JD, Lasaga AC (1991) Molecular-dynamics simulations of pressure and temperature effects on $MgSiO_3$ and Mg_2SiO_4 melts and glasses. Phys Chem Miner 17:661-673
Kubo R (1957) Statistical-mechanical theory of irreversible processes. i. general theory and simple applications to magnetic and conduction problems. J Phys Soc Japan 12:570-586

Lacks DJ, Rear DB, Van Orman JA (2007) Molecular dynamics investigation of viscosity, chemical diffusivities and partial molar volumes of liquids along the MgO-SiO_2 join as functions of pressure. Geochim Cosmochim Acta 71:1312-1323

Lange RA, Carmichael ISE (1987) Densities of Na_2O-K_2O-CaO-MgO-FeO-Fe_2O_3-Al_2O_3-TiO_2-SiO_2 liquids - new measurements and derived partial molar properties. Geochim Cosmochim Acta 51:2931-2946

Langevin P (1908) Sur la théorie du mouvement brownien. CR Acad Sci 146:530-533

Lasaga AC (1979) Multicomponent exchange and diffusion in silicates. Geochim Cosmochim Acta 43:455-469

Lasaga AC (1998) Kinetic Theory in the Earth Sciences, 1st Edition. Princeton University Press, Princeton, NJ

Lennard-Jones JE (1924) On the determination of molecular fields. II. From the equation of state of a gas. Proc R Soc A 106:463-477

Leslie M, Gillan MJ (1985) The energy and elastic dipole tensor of defects in ionic crystals calculated by the supercell method. J Phys C Solid State Phy 18:973-982

Liebske C, Schmickler B, Terasaki H, Poe P, Suzuki A, Funakoshi KI, Ando R, Rubie DC (2005) Viscosity of peridotite liquid up to 13 GPa: Implications for magma ocean viscosities. Earth Planet Sci Lett 240:589-604

Manning CE (2004) The chemistry of subduction-zone fluids. Earth Planet Sci Lett 223:1-16

Martin B, Spera FJ, Ghiorso MS, Nevins D (2009) Structure, thermodynamic and transport properties of liquid Mg_2SiO_4: Molecular dynamics simulations and model EOS. Am Mineral 94:693-703

Matsui M (1994) A transferable interatomic potential model for crystals and melts in the system CaO-MgO-Al_2O_3-SiO_2. Mineral Mag 58A:571-572

Matsui M, Anderson OL (1996) Molecular dynamics simulation of structures, bulk moduli, and volume thermal expansivities of silicate liquids in the system CaO-MgO-Al_2O_3-SiO_2.Geophys Res Lett 23:395-398

McQuarrie DA (1984) Statistical Mechanics. University Science Books, Sausalito, CA

Mermin ND (1965) Thermal properties of inhomogeneous electron gas. Phys Rev 137:1441

Merrill RT, McElhinny MW, McFadden PL (1998) The Magnetic Field of the Earth, 1st edition. Academic Press, London

Metropolis N, Rosenbluth AW, Rosenbluth MN, Teller AH, Teller E (1953) Equation of state calculations by fast computing machines. J Chem Phys 21:1087-1092

Mitrovica JX, Forte AM (2004) A new inference of mantle viscosity based upon joint inversion of convection and glacial isostatic adjustment data. Earth Planet Sci Lett 225:177-189

Mookherjee M, Stixrude L, Karki BB (2008) Hydrous silicate melt at high pressure. Nature 452:983-986

Nevins D, Spera FJ (1998) Molecular dynamics simulations of molten $CaAl_2Si_2O_8$: dependence of structure and properties on pressure. Am Mineral 83:1220-1230

Nevins D, Spera FJ, Ghiorso MS (2009) Shear viscosity and diffusion in liquid $MgSiO_3$: transport properties and implications for terrestrial planet magma oceans. Am Mineral 94:975-980

Nosé S (1984) A unified formulation of the constant temperature molecular dynamics methods. J Chem Phys 81:511-519

Nuevo MJ, Morales JJ, Heyes DM (1995) Mass dependence of isotope self-diffusion by molecular dynamics. Phys Rev E 51:2026-2032

Ohtaki H, Radnai T (1993) Structure and dynamics of hydrated ions. Chem Rev 93:1157-1204

Onsager L (1931a) Reciprocal relations in irreversible processes. I. Phys Rev 37:405-426

Onsager L (1931b) Reciprocal relations in irreversible processes. II. Phys Rev 38:2265-2279

Parrish RR (1985) Some cautions which should be exercised when interpreting fission-track and other dates with regard to uplift rate calculations. Nucl Tracks Radiation Measure 10:425

Payne MC, Teter MP, Allan DC, Arias TA, Joannopoulos JD (1992) Iterative minimization techniques for *ab initio* total-energy calculations - molecular-dynamics and conjugate gradients. Rev Mod Phys 64:1045-1097

Philibert J (1991) Atom Movements, Diffusion and Mass Transport in Solids, 1st Edition. Les Editions de Physique, Paris

Poirier JP (1988) Transport properties of liquid metals and viscosity of the Earth's core. Geophys J 92:99-105

Rahman A (1964) Correlation in the motion of atoms in liquid argon. Phys Rev 136:60-66

Reich M, Ewing RC, Ehlers TA, Becker U (2007) Low-temperature anisotropic diffusion of helium in zircon: Implications for zircon (U-Th)/He thermochronometry. Geochim Cosmochim Acta 71:3119-3130

Reid JE, Poe BT, Rubie DC, Zotov N, Wiedenbeck M (2001) The self-diffusion of silicon and oxygen in diopside ($CaMgSi_2O_6$) liquid up to 15 GPa. Chem Geol 174:77-86

Reiners PW, Spell TL, Nicolescu S, Zanetti KA (2004) Zircon (U-Th)/He thermochronometry: He diffusion and comparisons with $^{40}Ar/^{39}Ar$ dating. Geochim Cosmochim Acta 68:1857-1887

Richards M, Hager B (1984) Geoid anomalies in a dynamic earth. J Geoophys Res 89:5987-6002

Richter FM, Janney PE, Mendybaev RA, Davis AM, Wadhwa M (2007) Elemental and isotopic fractionation of type B CAI-like liquids by evaporation. Geochim Cosmochim Acta 71:5544-5564

Richter FM, Watson EB, Christensen JN, Hutcheon ID, Williams RW, Sturchio NC, Beloso AD Jr (2006) Kinetic isotopic fractionation during diffusion of ionic species in water. Geochim Cosmochim Acta 70:277-289

Richter FM, Watson EB, Mendybaev R, Dauphas N, Georg B, Watkins J, Valley J (2009) Isotopic fractionation of the major elements of molten basalt by chemical and thermal diffusion. Geochim Cosmochim Acta 73:4250-4263

Richter FM, Watson EB, Mendybaev R, Teng FZ, Janney PE (2008) Magnesium isotope fractionation in silicate melts by chemical and thermal diffusion. Geochim Cosmochim Acta 72:206-220

Rigden SM, Ahrens TJ, Stolper EM (1989) High-pressure equation of state of molten anorthite and diopside. J Geoophys Res 94:9508-9522

Rivers ML, Carmichael ISE (1987) Ultrasonic studies of silicate melts. J Geoophys Res 92:9247-9270

Ruff L, Anderson DL (1980) Core formation, evolution and convection: A geophysical model. Phys Earth Planet Inter 21:181-201

Rutter MD, Secco RA, Liu H, Uchida T, Rivers M, Sutton S, Wang Y (2002) Viscosity of liquid Fe at high pressure. Phys Rev B 66:060102

Sangster MJL, Stoneham AM (1984) calculation of absolute diffusion rates in oxides. J Phys C 17:6093-6104

Shewmon P (1989) Diffusion in Solids. Minerals, Metals & Materials Society, Warrendale, PA

Silvestrelli PL, Parrinello M (1999) Structural, electronic, and bonding properties of liquid water from first principles. J Chem Phys 111:3572-3580

Smigelskas AD, Kirkendall ED (1947) Zinc diffusion in alpha brass. Trans Am Inst Min Metall Eng 171:130-142

Smoluchowski M (1906) Essai d'une théorie cinétique du mouvement Brownien et des milieux troubles. Bull Int Acad Sci Cracovie p 577-602

Stebbins JF, Carmichael ISE, Moret LK (1984) Heat-capacities and entropies of silicate liquids and glasses. Contrib Mineral Petrol 86:131-148

Stixrude L, Bukowinski MST (1989) Compression of tetrahedrally bonded SiO_2 liquid and silicate liquid-crystal density inversion. Geophys Res Lett 16:1403-1406

Stixrude L, de Koker N, Sun N, Mookherjee M, Karki B (2009) Thermodynamics of silicate liquids in the deep Earth. Earth Planet Sci Lett 278:226-232

Stixrude L, Karki BB (2005) Structure and Freezing of $MgSiO_3$ liquid in the Earth's lower mantle. Science 310:297-299

Terasaki H, Kato T, Urakawa S, Funakoshi K, Sato K, Suzuki A, Okada T (2002) Viscosity change and structural transition of molten Fe at 5 GPa. Geophys Res Lett 29:1227

Tonks WB, Melosh HJ (1993) Magma ocean formation due to giant impacts. J Geoophys Res 98:5319-5333

Tosi N, Čadek O, Martinec Z (2009) Subducted slabs and lateral viscosity variations: effects on the long-wavelength geoid. Geophys J Int 179:813-826

Tossel JA (2005) Theoretical study on the dimerization of $Si(OH)_4$ in aqueous solution and its dependence on temperature and dielectric constant. Geochim Cosmochim Acta 69:283-291

Urey HC (1955) The cosmic abundances of potassium, uranium and thorium and the heat balances of the Earth, the Moon, and Mars. Proc Nat Acad Sci USA 41:127-144

van Beest BWH, Kramer GJ, van Santen RA (1990) Force fields for silicas and aluminophosphates based on ab initio calculations. Phys Res Lett 64:1955-1958

Verlet L (1967) Computer "experiments" on classical fluids. I. thermodynamical properties of Lennard-Jones molecules. Phys Rev 159:98-103

Vinyard GH (1957) Frequency factors and isotope effects in solid state rate processes. J Phys Chem Solids 3:121-127

Vočadlo L (2007) Mineralogy of the Earth - The Earth's core: iron and iron alloys. *In:* Treatise of Geophysics, Volume 2: Mineral Physics. Price G (ed) Elsevier, p 91-120

Vočadlo L, de Wijs GA, Kresse G, Gillan M, Price GD (1997) First principles calculations on crystalline and liquid iron at Earth's core conditions. Faraday Discuss 106:205-217

Vočadlo L, Wall A, Parker SC, Price GD (1995) Absolute ionic diffusion in MgO - computer calculations via lattice dynamics. Phys Earth Planet Inter 88:193-210

Wheeler DR, Newton J (2004) Molecular dynamics simulations of multicomponent diffusion. 1. equilibrium method. J Phys Chem 108:18353-18361

Willeke M (2003) Limits of the validity of the mass ratio independence of the Stokes-Einstein relation: molecular dynamics calculations and comparison with the Enskog theory. Molec Phys 101:1123-1130

Wood WW, Parker FR (1957) Monte Carlo equation of state of molecules interacting with the Lennard-Jones potential. I. A supercritical isotherm at about twice the critical temperature. J Chem Phys 27:720-733

Wright K, Price G (1993) Computer simulations of defects and diffusion in perovskites. J Geoophys Res 98:22245-22253

Yeh IC, Hummer G (2004) System-size dependence of diffusion coefficients and viscosities from molecular dynamics simulations with periodic boundary conditions. J Phys Chem B 108:15873-15879

Zhang Y (2008) Geochemical Kinetics. Princeton University Press, Princeton, NJ

Zhang Y (2010) Diffusion in minerals and melts: theoretical background. Rev Mineral Geochem 72:5-59

Zhang Y, Guo G, Refson K, Zhao Y (2004) Finite-size effect at both high and low temperatures in molecular dynamics calculations of the self-diffusion coefficient and viscosity of liquid silica. J Phys Condens Matter 16:9127-9135

Zhou Y, Miller GH (1996) Green-Kubo formulas for mutual diffusion coefficients in multicomponent systems. J Phys Chem 100:5516-5524

Zwanzig R (1965) Time-correlation functions and transport coefficients in statistical mechanics. Annu Rev Phys Chem 16:67-102